Nanoporous Materials

DOI: 10.1002/anie.201108915

Chemical-Assisted Thermal Disproportionation of Porous Silicon Monoxide into Silicon-Based Multicomponent Systems**

Jung-In Lee, Kyu Tae Lee, Jaephil Cho, Jeyoung Kim, Nam-Soon Choi, and Soojin Park**

Commercially available silicon monoxide is an unstable material at high temperatures (> 1000 °C), at which point it disproportionates to silicon nanocrystals and amorphous silicon suboxides.[1,2] The nanostructuring of SiO, or its conversion to Si, has been carried out using several approaches, such as mechanical milling,[3] chemical vapor deposition,[4] and reduction by elemental metals at high temperatures (> 900 °C).[5] However, these methods did not retain the original morphology of the SiO. Herein, we demonstrate a process for fabricating three-dimensional nanoporous SiO by metal-assisted chemical etching, without changing the chemical and physical properties of the original materials. Subsequent chemical-assisted thermal annealing led to the conversion of porous SiO into shape-preserving Si-based multicomponent systems that consisted of core (Si dispersed in amorphous silicon suboxides) and shell (crystalline silica). Small amounts of alkaline solutions induced the crystallization of amorphous silica into crystalline silica, and simultaneously assisted the disproportionation at a modest temperature (> 700 °C). We used the porous SiO and the Si-based systems as anode materials in lithium-ion batteries. These systems exhibited a high reversible capacity (ca. 1600 mA h g^{-1}) and a stable retention over 100 cycles. The chemical-assisted thermal disproportionation is simple, low in costs, and mass-productive (high yield of > 99 % on a scale of tens of grams per batch), and thus, opens up an effective way to produce high-performance anode materials. In addition, the nanostructuring of SiO by the above-mentioned process may be extended to a wide variety of applications, such as optoelectronics,[6] solar cells,[7] antireflection coatings,[8] and lithium-ion batteries.[3]

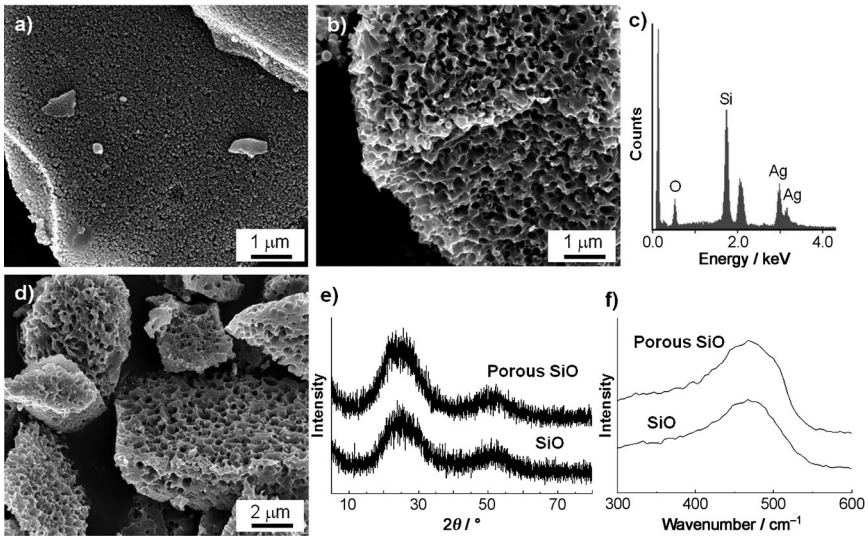

Figure 1. Three-dimensional porous SiO prepared by Ag-catalytic chemical etching. a) Scanning electron microscope (SEM) image of Ag-deposited SiO obtained by galvanic reaction. b) SEM image of SiO that was chemically etched by Ag catalyst. c) Energy-dispersive X-ray analysis of chemically etched SiO (b). d) SEM image of 3D porous SiO produced by selective dissolution of Ag in concentrated HNO_3 solution. e) X-ray diffraction patterns of pristine (bottom) and porous SiO (top). f) Raman spectra of pristine (bottom) and porous SiO (top).

We used commercially available bulk SiO (Aldrich) with an average particle size of 20 μm to prepare three-dimensional (3D) nanoporous SiO structures through a metal-assisted chemical etching process. First, Ag nanoparticles were deposited onto SiO surfaces by galvanic displacement reactions from a mixture of $AgNO_3$ (3 mM) and HF (5 M; Figure 1 a). Second, the Ag-deposited SiO particles were immersed in a chemical etchant, a mixture of HF (5 M) and H_2O_2 (0.3 M), to etch the SiO layer beneath the Ag layer and result in the formation of nanopores (Figure 1 b). Energy dispersive X-ray analysis indicated that etched SiO contains Si, O, and Ag nanoparticles (Figure 1 c). Subsequently, the Ag particles were completely removed in concentrated nitric acid to obtain the 3D porous SiO structures (Figure 1 d). The X-ray diffraction (XRD) pattern and Raman spectrum of porous SiO show typical characteristics of amorphous SiO, which are the same as those of the commercially available bulk SiO material (Figure 1 e, f). It should be noted that the chemical and physical properties of chemically etched SiO materials remained unchanged, except for the formation of nanopores on the surface and inside the SiO layer. To the best

[*] J.-I. Lee, Prof. K. T. Lee, Prof. J. Cho, Prof. N.-S. Choi, Prof. S. Park
Interdisciplinary School of Green Energy, UNIST
Ulsan, 689-798 (South Korea)
E-mail: nschoi@unist.ac.kr
spark@unist.ac.kr
Dr. J. Kim
LG Chem, Ltd., Daegeon, 305-380 (South Korea)

[**] This work was supported by the Converging Research Center Program (2011K000637) and the MKE/ITRC program of NIPA (NIPA-2012-C1090-1200-0002).

Supporting information for this article is available on the WWW under http://dx.doi.org/10.1002/anie.201108915.

of our knowledge, synthesis of nanoporous SiO materials from bulk SiO particles was not reported previously.

Commercially available amorphous, solid SiO is technically prepared from Si and SiO_2 at high temperatures by condensation of gaseous SiO, which has a similar electronic structure to CO.[1,2] The atomic structure of solid SiO is still controversial, despite a number of physical and chemical investigations. Philipp suggested the random-bonding model (RB model), a statistical mixture of Si–Si and Si–O bonds.[9] Another model is the random-mixture model (RM model, microscropic-mixture model), in which Si and SiO_2 particles with sizes of a few nanometers are connected by a region with an intermediate stoichiometry.[10] Spectroscopic and structural characterizations of commercially available SiO have been extensively investigated. RB and RM models were modified to a more realistic model that is the mixed-phase model with different bond accumulations, that is, regions with an accumulation of Si–Si bonds and regions with an accumulation of Si–O bonds are present.[11]

When solid SiO powders were immersed in HF (5 M) for one hour, a rough surface was observed with features, the size of which ranged from a few nanometers to tens of nanometer. Because Si–O bond-rich regions were selectively etched by HF solution, the rough surface was obtained and the oxygen contents (24 %) were significantly decreased, thus indicating the mixed-phase model (see the Supporting Information, Figure S1). In contrast, metal-assisted chemical etching happens without changing the chemical and physical properties of SiO particles. The working principle of the metal-assisted chemical etching is similar to the formation in an Si wafer.[12] Metal (e.g., Ag, Au, Cu, or Pt) particles act as a local cathode, while the Si–Si bond-rich surface of SiO serves as an anode. SiO is dissolved continuously by transferring electrons to the Ag particles at the interface of the metal and Si, while oxidation of Ag particles by H_2O_2 and reduction of Ag^+ ions take place on the cathode. In this manner, the SiO layer that is in contact with the Ag particles is continuously etched down to give 3D porous structures. The size of the Ag nanoparticles was determined by galvanic reaction time. When the SiO powders were immersed in $AgNO_3$ (3 mM) and HF (5 M) for ten minutes, tens of nanometers of Ag nanoparticles were deposited onto the surface of the SiO layer (Figure 1 a). Subsequent immersion of Ag-deposited SiO in chemical etchant (HF/H_2O_2 mixture) for 30 minutes formed the Ag-embedded 3D porous SiO structures (Figure 1 b). It should be noted that the size of Ag nanoparticles was increased during the chemical etching, because the Ag particles have a strong tendency to aggregate with neighboring Ag particles in a chemical etchant.[13] The Ag nanoparticles can be removed by immersion in concentrated HNO_3 at 50 °C for two hours (Figure 1 d). The corresponding cross-sectional SEM image showed that the chemical etching of SiO occurred to the center of the particles (Supporting Information, Figure S2).

Nitrogen adsorption (Brunauer–Emmett–Teller, BET) measurements indicated that the specific surface areas of commercially available bulk SiO and the 3D porous SiO were 1.5 $m^2 g^{-1}$ and 46 $m^2 g^{-1}$, respectively. Barrett–Joyner–Halenda (BJH) analyses[14] of the nitrogen desorption curves indicated that the porous SiO possessed a large amount of nanopores (tens of nanometers in diameter) and a small amount of macropores (hundreds of nanometers in diameter; Supporting Information, Figure S3). When the concentration of H_2O_2 was decreased to 0.1 M, the specific surface areas of the porous SiO was 17 $m^2 g^{-1}$, thus indicating that the amount of H_2O_2 plays an important role in the formation of mesopores inside the SiO materials. The H_2O_2 concentration determines the concentration of Ag^+ ions. When a large amount of H_2O_2 is used to etch the SiO layer, the Ag^+ ions that are not recovered into the original Ag nanoparticles may start to deposit onto certain defective sites and etch the SiO layer beneath in order to form mesopores.[15]

Solid SiO is well known to be thermally unstable at temperatures higher than 450 °C and disproportionate to Si and SiO_2.[16] When a commercially available SiO sample was thermally annealed at more than 1000 °C for several hours, the disproportionation reaction took place, in which Si nanocrystals were randomly dispersed within an amorphous SiO_2 matrix. In contrast, the use of NaOH as a catalyst enabled the disproportionation of SiO to be conducted at a much lower temperature and in a shorter period of time. At this point, a multicomponent Si-based alloy consisting of a core (crystalline Si randomly dispersed in a SiO_x matrix) and shell (crystalline SiO_2, cristobalite) was formed with a high yield of more than 99 %. When a mixture of SiO and NaOH was heated at 800 °C for one hour, the resulting Si-based product (Figure 2 a) retained the morphology of the original 3D porous SiO. The XRD analysis indicated that crystalline Si, cristobalite, and amorphous SiO_x phases were formed after thermal annealing at a modest temperature (Figure 2 b). Previously, Bao et al. reported the conversion of 3D crystal-

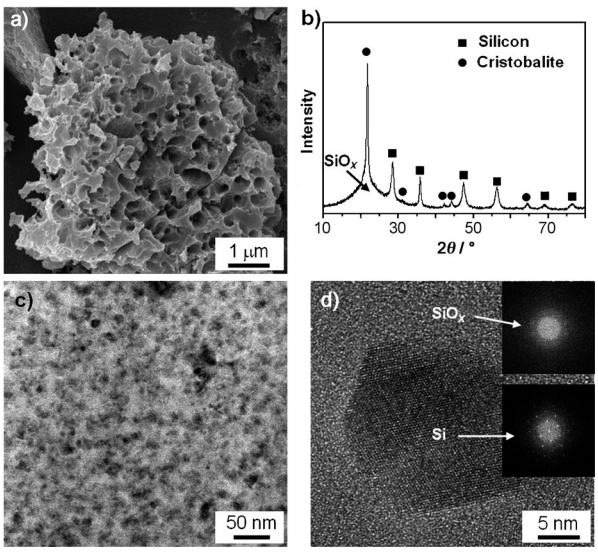

Figure 2. 3D porous Si-based multicomponent system prepared by chemical-assisted thermal disproportionation of porous SiO. a) SEM image of porous Si-based multicomponent system. b) XRD patterns of crystalline Si, amorphous SiOx, and cristobalite (crystalline SiO_2). c) Cross-sectional TEM image of crystalline Si (dark spots) and amorphous SiOx (gray regions). d) HR-TEM image of the crystalline Si and amorphous SiO_x seen in (c). Insets in (d) show the Fourier-transformed patterns that indicate an amorphous characteristic of SiO_x (top) and a typical crystalline Si (bottom).

line silica into shape-preserving Si by a magnesiothermic reduction process.[17] However, chemical reduction of amorphous porous silica did not retain the original morphologies. The chemical-assisted thermal annealing process enabled us to synthesize shape-preserved porous Si-based materials from amorphous SiO particles.

The transmission electron image of cross-sections of the Si-based alloy shows crystalline Si (crystal size of ca. 10 nm) randomly dispersed in an SiO_x matrix (Figure 2c). The corresponding HR-TEM image confirmed a highly crystalline Si and an amorphous SiO_x phase (Figure 2d). The x value in the SiO_x phase is close to 1, as shown by numerous EDAX results (Supporting Information, Figure S4).

To investigate the effects of the NaOH catalyst, the reaction temperature, and the reaction time on the disproportionation of SiO, the weight ratio of SiO and NaOH was fixed at 20:1. When a mixture of SiO and NaOH was heated to several different temperatures within one hour, the disproportionation of SiO into Si and SiO_2 was initiated at 700 °C. As the temperature was increased to 900 °C, the peak intensities of crystalline Si and cristobalite were significantly increased, while SiO_x peaks markedly decreased (Figure 3a). The solid SiO was significantly disproportionated by heating at 900 °C for one minute or by increasing the amount of

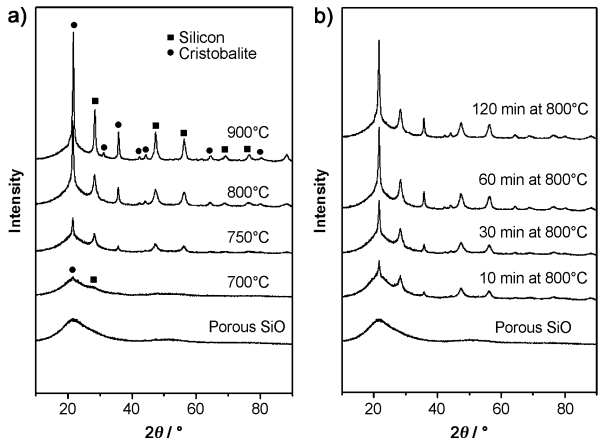

Figure 3. XRD patterns of disproportionated porous SiO at various temperatures and annealing times. a) XRD patterns showing disproportionation of SiO at different annealing temperatures with a fixed reaction time of 1 h. b) XRD patterns showing relative amounts of Si, SiO_x, and cristobalite at various annealing times with a fixed temperature of 800 °C.

NaOH (Supporting Information, Figure S5). It should be noted that the disproportionation of SiO did not occur without NaOH, even by heating the sample at 900 °C for several hours. In addition, as the mixture of SiO and NaOH was annealed at a fixed temperature (800 °C), the amounts of Si and cristobalite increased with time (Figure 3b). From the peak areas of XRD patterns (Figure 3b), we confirmed that the contents of Si and SiO_2 were significantly increased with time, while the SiO_x phase decreased (Supporting Information, Figure S6). The corresponding Raman spectra show the crystalline characteristics of as-synthesized Si at various annealing times, thus indicating that the amount and crystallinity of Si can be tuned by controlling the reaction temperature and time (Supporting Information, Figure S6b). The crystal size of the cristobalite was calculated by Scherrer analysis of the XRD data.[18] The crystal size increased with increasing annealing time and annealing temperature (Supporting Information, Figure S7).

Next, we investigated the spatial locations of crystalline SiO_2 (cristobalite) in the Si-based alloy. The cross-section was obtained from a focused ion beam that made use of Ga ions to etch away a sample with a high spatial precision. TEM analysis of the cross-section indicated that the cristobalite was located in the outer shell, and the thickness of SiO_2 increased with reaction time. It should be noted that the cristobalite phase is very sensitive to the electron beam (that is, it is melted by beam exposure within a few seconds), so that the selected area diffraction patterns of the crystalline silica was instantly obtained (Supporting Information, Figure S8). As further evidence of the SiO_2 in the outer shell, we employed time-of-flight secondary ion mass spectrometry to obtain the contour map of Si and SiO_2. The as-synthesized Si-based alloy showed that the SiO_2 phases were clearly located on the top surface. After depth profiling (etching rate of 11 nm min^{-1} for SiO_2 layer), the intensities of Si phases were much stronger than those of SiO_2, thus indicating that most SiO_2 layers were etched away in the SiO sample that reacted at 800 °C for 30 minutes (Supporting Information, Figure S9).

From these results, we proposed the mechanism of disproportionation of solid SiO into Si, SiO_x, and cristobalite through chemical-assisted thermal annealing. Initially, NaOH is uniformly coated onto the surface of SiO. During the thermal annealing process, NaOH assisted the disproportionation of SiO into Si and amorphous silica (SiO_2) and simultaneously induced the crystallization of amorphous silica in the outer shell to crystalline silica. The high-temperature annealing of amorphous SiO_2 in the presence of alkaline solutions led to the formation of crystalline SiO_2.[19] As the annealing time increased, oxygen from Si–O bond-rich regions in the inner phases was transported to the outer layer, resulting in an increased cristobalite phase in the shell regions, while the size of Si nanocrystals in the inner regions was increased because of the coagulation of the oxygen-deficient regions. At the same time, amorphous SiO_x phases were gradually decreased as a function of reaction time. Zhang et al. reported a similar mechanism by using a density-functional calculation; the oxygen atoms in the larger SiO clusters preferred to migrate from the centers to the outer surfaces, thus leading to the growth of Si cores.[20]

These Si-based materials have been used as alternative anode materials for lithium-ion batteries (LIBs) because of their high theoretical specific capacity (3580 mA h g^{-1} for $Li_{15}Si_4$, compared to commercialized graphite of 372 mA h g^{-1}).[21–24] However, pure Si has not yet been used in commercial LIBs, owing to the mechanical failure caused by formidable large-volume expansion during battery operation, resulting in the desquamation of active materials from the current collector upon prolonged cycles. To overcome these problems, the SiO or disproportionated SiO materials can be used. The SiO electrodes appeared particularly

promising in LIBs because of their higher reversible capacity ($>800\ mA\,h\,g^{-1}$) and long cycle life (>100 cycles).[3]

The 3D porous SiO- and Si-based alloy electrodes have been used as anode materials in LIBs. To improve the electrochemical conductivity of Si-based materials, a carbon layer (ca. 6 wt%) was coated onto the surface of electrode materials by using a well-known thermal decomposition process (800 °C for 20 min) of acetylene gas (Figure 4a).[25] The high specific surface areas and porous structures of both

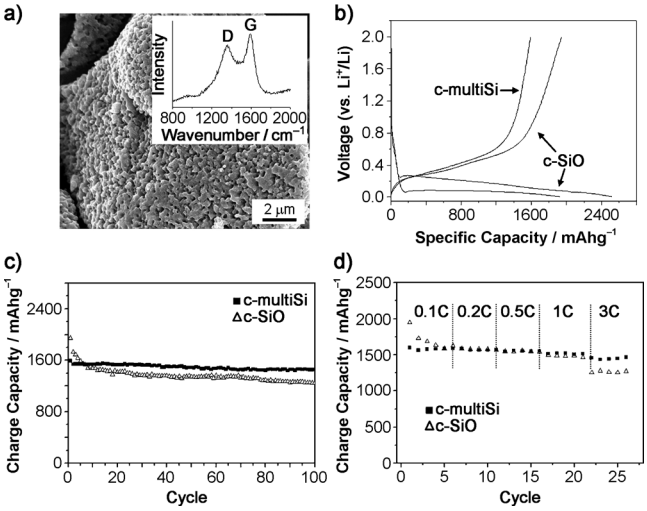

Figure 4. Electrochemical performances of c-SiO and c-multiSi electrodes. a) SEM image of carbon-coated Si-based multicomponent system obtained by reaction at 800 °C for 30 min; inset: Raman spectrum of the carbon layer, indicating characteristics of amorphous carbon (with D/G ratio of 1.66). b) Voltage profiles, and c) cycling retention of c-SiO and c-multiSi obtained at a rate of 0.1 C between 2.0 V and 0.005 V. d) Rate capabilities of c-SiO and c-multiSi. The discharge was fixed at a rate of 0.1 C.

3D nanoporous electrode materials are attractive characteristics for use as anode materials in LIBs. To evaluate such electrochemical performances, coin cells (2016 type) with a metallic-lithium counter electrode were operated. The voltage profiles of carbon-coated porous SiO (c-SiO) and carbon-coated Si-based multicomponent electrodes (c-multiSi, sample annealed at 800 °C for 30 min) were obtained at a rate of 0.1 C between 2.0 V and 0.005 V (Figure 4b). The first-cycle discharge capacities are 2520 and 1930 $mA\,h\,g^{-1}$ for the electrodes of c-SiO and c-multiSi, with the corresponding coulombic efficiency of 77.3 and 82.8%, respectively. Since Si-based materials without carbon-coating have a low electrochemical conductivity, a low coulombic efficiency at the first cycle was exhibited (Supporting Information, Figure S10). To the best of our knowledge, the coulombic efficiency of c-multiSi electrode is the highest value among SiO-based materials.[25–27] The high value of the coulombic efficiency at the first cycle is attributed to several reasons. First, a thin carbon layer minimizes the direct contact between the c-multiSi and the electrolyte, and promotes the formation of a stable solid electrolyte interphase (SEI) layer on the surface of the porous electrodes. Second, the cristobalite layer in the outer shells of c-multiSi contributes to a specific capacity, and it may also make a dense SEI layer (Supporting Information, Figure S11). Third, the 3D porous structure offers a pathway for the efficient access of electrons and electrolytes. Moreover, the stable cycle performance of c-multiSi may be attributed to the carbon-coating effect and buffer layers (cristobalite in the outer shell and amorphous SiO_x matrix in the core), which alleviate the volume expansion during battery operation. Capacity retention of c-multiSi electrodes after 100 cycles was 91.3% at the rate of 0.1 C, while the c-SiO showed a poor cycle retention of 51.9% (Figure 4c). In the case of c-SiO, the oxide is irreversibly reduced with the formation of nanoclusters of amorphous Si surrounded by Li_2O matrix during the first cycle, resulting in a huge fading of capacity. However, after the initial irreversible reaction, a stable cycle retention was seen. Moreover, the c-multiSi and the c-SiO showed excellent high-rate capabilities of 90% and 65% at a rate of 3 C, respectively, compared to those at a rate of 0.1 C (Figure 4d). Since an increased specific surface area of the porous Si-based multicomponent system enhances accessibility of lithium ions and electrolytes, high rate capabilities were exhibited, compared to bare SiO electrodes (Supporting Information, Figure S12). These results indicated that both the porous structure and the multicomponent system of electrodes played an important role in determining the electrochemical performance in LIBs.

In summary, the present work demonstrates that 3D nanoporous SiO can be synthesized with a yield of 30–40% by the metal-assisted catalytic etching process at room temperature, without changing the chemical and physical properties of commercially available SiO. Subsequently, the nanoporous SiO can be converted to a shape-preserving Si-based multicomponent system (with a high yield of more than 99%) through chemical-assisted thermal disproportionation at 700–900 °C. These methods are scalable approaches, which can produce tens of grams of samples per batch in a laboratory. The nanoporous SiO- and Si-based multicomponent system can provide high-performance electrochemical properties, including a high specific reversible capacity (ca. $1600\ mA\,h\,g^{-1}$) and a stable cycle retention (100 cycles), as promising anode materials in LIBs. Also, the concepts of nanostructuring of SiO materials and shape-preserving chemical conversion can be extended to other Si-based materials for use in electronic, optical, or other applications.[3,6–8]

Experimental Section

Synthesis of 3D nanoporous SiO. SiO (325 mesh) was purchased from Aldrich. For a galvanic displacement reaction, SiO powder was immersed in a solution of $AgNO_3$ (3 mM) and HF (5 M) at room temperature for 5 min to uniformly deposit a silver layer onto the surface of the SiO particles. Subsequently, excess silver salts were removed by rinsing the Ag-deposited SiO powder in a large amount of deionized water for several times. Immediately after filtering, the powder was immersed in a chemical etchant consisting of HF (5 M) and H_2O_2 (0.1–0.3 M) at room temperature for 30 min, to obtain nanoporous SiO particles. The specific surface area of etched SiO could be tuned by controlling the concentration of H_2O_2. After chemical etching, Ag nanoparticles were completely removed by concentrated HNO_3 at 50 °C for 2 h, rinsed with a copious amount of deionized water, and then dried in a vacuum oven at 80 °C for 12 h.

Conversion of SiO to Si-based multicomponent system. SiO powder (2 g) and NaOH (0.5 g) were mixed in EtOH (20 mL) and stirred for 3 h. After removing EtOH, the mixture of SiO and NaOH was placed inside an alumina boat and transferred to a tube furnace. The pressure was reduced to 10^{-3} Torr and the furnace was heated to the target temperature (700–900 °C) at a rate of 5 °C min^{-1} under an argon stream, and then kept at this temperature for a certain period of time. After thermal reaction of the sample mixture, it was cooled down to room temperature. The as-synthesized samples were rinsed with deionized water or EtOH to remove residual unreated NaOH. Under these conditions, nanoporous SiO was converted to shape-preserving Si-based multicomponent system.

Characterization of the porous SiO- and Si-based multicomponent system. The crystal structures of SiO, porous SiO, and disproportionated SiO were measured by a high-power X-ray diffractometer (XRD) on a Rigaku D/MAX at 2500 V using Ni-filtered $Cu_{K\alpha}$ radiation. Raman spectra were recorded on a JASCO spectrometer (NRS 3000) to confirm the characteristics of Si and SiO. Also, the degree of graphitization of a carbon coating layer in the sample was determined. A He–Ne laser as the excitation source was operated at 632.8 nm. The focused ion beam (Quanta 3D FEG) was operated using Ga ions to enable cross-section processing of disproportionated SiO samples. The transmission electron microscope (TEM) was employed to investigate the cross-section. TEM images were taken in the bright-field mode using JEM-1400 (JEOL) operating at an accelerating voltage of 200 kV. SiO- and Si-based multicomponent systems were characterized by a scanning electron microscope (SEM, NanoSEM 230, FEI) operating at 5 kV with a 3 nm thick platinum-coating layer. The nitrogen adsorption and desorption isotherms were measured with a VELSORP-mini II (BEL Japan, Inc.) at 77 K in the relative pressure range of P/P_0 from 0.05 to 0.3. It was fitted to the Brunauer–Emmett–Teller (BET) equation to determine the specific surface areas.

Electrochemical properties of Si electrodes. For the electrochemical properties, coin-type half cells (2016 R-type) were prepared with Si powders (as the working electrode) and lithium metal (as counter-electrode) under an argon-filled glove box. The electrode for the electrochemical test was made of active material (60 wt %), super P carbon black (20 wt %), and poly(acrylic acid)/sodium carboxymethyl cellulose (wt/wt = 50/50) binder (20 wt %). The electrolyte was $LiPF_6$ (1.3 M) with ethylene carbonate/diethylene carbonate (EC/DEC, 30:70 vol %) and 5 wt % fluorinated ethylene carbonate additive. The coil cells were cycled at a rate of 0.1–3 C between 0.005 V and 2.0 V.

Received: December 18, 2011
Published online: February 3, 2012

Keywords: nanoporous materials · multicomponent systems · silicon · silver · thermal disproportionation

[1] G. Hass, *J. Am. Ceram. Soc.* **1950**, *33*, 353.
[2] A. Hohl, T. Wieder, P. A. van Aken, T. E. Weirich, G. Denninger, M. Vidal, S. Oswald, C. Deneke, J. Mayer, H. Fuess, *J. Non-Cryst. Solids* **2003**, *320*, 255.
[3] J. H. Kim, H. J. Sohn, H. Kim, G. Jeong, W. Choi, *J. Power Sources* **2007**, *170*, 456.
[4] F. M. Kolb, H. Hofmeister, R. Scholz, M. Zacharias, U. Gösele, D. D. Ma, S.-T. Lee, *J. Electrochem. Soc.* **2004**, *151*, G472.
[5] E. Biehl, U. Schubert, F. Kubel, *New J. Chem.* **2001**, *25*, 994.
[6] G. Hass, C. D. Salzberg, *J. Opt. Soc. Am.* **1954**, *44*, 181.
[7] V. Kapaklis, C. Politis, P. Poulopoulos, P. Schweiss, *Appl. Phys. Lett.* **2005**, *87*, 123114.
[8] K. W. Wecht, *Appl. Opt.* **1991**, *30*, 4133.
[9] H. R. Philipp, *J. Non-Cryst. Solids* **1972**, *8–10*, 627.
[10] R. J. Temkin, *J. Non-Cryst. Solids* **1975**, *17*, 215.
[11] E. Füglein, U. Schubert, *Chem. Mater.* **1999**, *11*, 865.
[12] T. Qiu, P. K. Chu, *Mater. Sci. Eng. R* **2008**, *61*, 59.
[13] K. Peng, Y. Wu, H. Fang, X. Zhong, Y. Xu, J. Zhu, *Angew. Chem.* **2005**, *117*, 2797; *Angew. Chem. Int. Ed.* **2005**, *44*, 2737.
[14] E. P. Barrett, L. G. Joyner, P. P. Halenda, *J. Am. Chem. Soc.* **1951**, *73*, 373.
[15] Y. Qu, L. Liao, Y. Li, H. Zhang, Y. Huang, X. Duan, *Nano Lett.* **2009**, *9*, 4539.
[16] J. A. Yasaitis, R. Kaplow, *J. Appl. Phys.* **1972**, *43*, 995.
[17] Z. Bao, M. R. Weatherspoon, S. Shian, Y. Cai, P. D. Graham, S. M. Allan, G. Ahmad, M. B. Dickerson, B. C. Church, Z. Kang, H. W. Abernathy III, C. J. Summers, M. Liu, K. H. Sandhage, *Nature* **2007**, *446*, 172.
[18] B. D. Cullity, *Elements of X-Ray Diffraction*, Addison-Wesley, Reading, MA, **1978**.
[19] W. S. Fyfe, S. McKay, *Am. Mineral.* **1962**, *47*, 83.
[20] R. Q. Zhang, M. W. Zhao, S. T. Lee, *Phys. Rev. Lett.* **2004**, *93*, 095503.
[21] T. D. Hatchard, J. R. Dahn, *J. Electrochem. Soc.* **2004**, *151*, A838.
[22] G.-A. Nazri, G. Pistoia, *Lithium Batteries: Science and Technology*, Kluwer Academic/Plenum, Boston, **2004**.
[23] C. K. Chan, H. Peng, G. Liu, K. McIlwrath, X. F. Zhang, R. A. Huggins, Y. Cui, *Nat. Nanotechnol.* **2008**, *3*, 31.
[24] A. Magasinski, P. Dixon, B. Hertzberg, A. Kvit, J. Ayala, G. Yushin, *Nat. Mater.* **2010**, *9*, 353.
[25] U. Kasavajjula, C. Wang, A. J. Appleby, *J. Power Sources* **2007**, *163*, 1003.
[26] C.-M. Park, W. Choi, Y. Hwa, J.-H. Kim, G. Jeong, H.-J. Sohn, *J. Mater. Chem.* **2010**, *20*, 4854.
[27] X. Yang, Z. Wen, X. Xu, B. Lin, S. Huang, *J. Power Sources* **2007**, *164*, 880.

